AN APPROXIMATE RIEMANN SOLVER FOR TWO LAYER SHALLOW WATER EQUATIONS IN HORIZONTAL CENTRIFUGAL CASTING

J. Bohacek[1], A. Kharicha[1*], A. Ludwig[1], M. Wu[1,2], A. Paar[3], M. Brandner[3], L. Elizondo[3], T. Trickl[3]

[1] Chair of Simulation and Modelling of Metallurgical Processes, Montanuniversitaet Leoben, Austria

[2] Christian Doppler Laboratory for Advanced Process Simulation of Solidification and Melting, Montanuniversitaet Leoben, Austria

[3] Research & Development, Eisenwerk Sulzau-Werfen, R. & E. Weinberger AG, Austria

[*] Corresponding author: abdellah.kharicha@unileoben.ac.at

s

ABSTRACT

An approximate Riemann solver was developed for solving the shallow water equations (SWE) and energy transport describing the average flow dynamics of two liquid layers spreading inside a horizontally rotating cylinder. The numerical model was particularly developed for simulating the horizontal centrifugal casting (HSC) of the outer layer and the intermediate layer of a work roll. The SWE were derived in the rotating frame of reference; therefore, fictitious forces (the centrifugal force and the Coriolis force) were considered. In addition, other forces such as the bed shear force, the force of gravity, and forces arising from the variable liquid/solid interface were taken into account. The mould filling was realized through a Gaussian mass source applied in the centre of the mould. In addition to the flow solver, the enthalpy equation with the appropriate boundary conditions was solved inside the mould, end cores, and the casting. The solidification progress was studied by means of plotting the time dependent solid shell thickness at selected locations. The calculations were successfully validated with the pyrometer and thermo-camera measurements.

KEYWORDS

steel, centrifugal casting, numerical modelling, shallow water equations, mould filling

INTRODUCTION

In the present paper a numerical simulation of the horizontal centrifugal casting (HSC) of the outer layer and the intermediate layer of a work roll is concerned. In short, the HSC process can be outlined as the following: An initially empty cylindrical mould is from inside painted with the refractory material and laid on four carrying rollers, from which two coaxial rollers are driven and the other two are driving. Prior to the casting, the mould is preheated to a desired temperature and the driving rollers gradually bring the mould into the rotational motion. When the desired rounds per minutes is reached the casting of the outer shell can start. A liquid metal is poured from the crucible via the statically mounted runner approximately in the centre of the mould. Due to high centrifugal forces ($>100g$) the liquid metal spreads uniformly and generates a sleeve of constant thickness. The solidification front proceeds from the relatively cold wall of the mould. After some period of time, the outer layer is partially solidified and the pouring of the intermediate layer begins. The centrifuging continues until the solidification is completed inside both layers.

Among other research papers published recently, numerical models differ mainly in whether the flow was solved or not. All research papers we mention here deal with a single layer casting i.e., in none of them the casting of two layers is discussed. Most of the numerical studies solving the flow dynamics used the VOF method [1] to capture the interface between the melt and the surrounding air. Xu [2] introduced an interesting numerical model of the HSC process. The full set of Navier-Stokes equations was solved along with the heat advection-diffusion equation. The main focus of the paper dwells in

studying different gating systems for the filling. Simulations were terminated at 30 seconds, when the filling was completed. The solidification model is not discussed in the paper. Next interesting paper on the HSC process namely on the centrifugal casting of seamless pipes was written by Kaschnitz [3]. In this case, a commercial package FLOW-3D was used. In order to avoid extremely small time steps, momentum equations were solved in the rotating frame of reference. However, due to a very small wall-to-length thickness ratio, one simulation still took considerably long time (~20 days).

A commercial package (STAR-CD V4) was also used in a paper by Keerthiprasad [4]. An effort was spent on comparing the cold flow simulations of the single layer HSC with the experimental castings. The mesh inside the mould was entirely constructed out of rather coarse polyhedral elements, which allowed notably large time steps (~0.01 s). Only the continuity and momentum equations were solved for the flow. Heat transfer and solidification were not discussed in the paper.

Results from simulations showed roughly how the melt is spreading during the filling stage, however no details are given on how the filling was imposed and whether the model could capture some free surface patterns or not. From the literature survey it can be concluded that when the main objective of the research paper is a simulation of the free-surface, the heat transfer and the solidification are usually ignored. The main reason for this is different characteristic times for the free-surface motion and the solidification. In addition to free-surface simulations, several research papers can be listed, which neglect the flow, do not consider mould filling, or assume a static flat free-surface. Such works generally target on simulation of the solidification of the whole liquid layer, very often accompanied by a segregation of some element due to a density difference and extremely high centrifugal pressure. For example in [5], Drenchev introduced a numerical model discussing some aspects of macrosegregation of reinforcing particles in a metal matrix. The enthalpy equation was the primary equation to solve with thermal physical properties determined from the segregation model. Since the flow (or the mould filling) was not included, the initial thickness of the liquid layer

was uniform and identical to the final thickness of the shell. Similar numerical models can be found in [6, 7]. The main bottleneck is the fact that the model lacks variances in the mould and shell temperatures due to the localized filling, which in turn affects the local thickness of the solidified shell and the macrostructure pattern consequently.

In the present paper, we introduce a novel approach for modelling of average flow dynamics of both, the outer and the intermediate, layers. These two layers are immiscible. Here, the two layer model is an extension of the single layer model detailed e.g. in [8, 9]. Moreover, the top layer has lower density than the bottom layer. Instead of solving the full set of Navier-Stokes equations with the advection equation for the volume fraction (VOF method), which is inherently computationally expensive, we make assumption that the flow obeys so-called two layer shallow water equations (SWE). The flow during the HSC process can be characterized as a free surface flow with the moving interface between two layers, in which the thickness of each layer is rather small compared to the length of the mould. For this reason, it is rational to expect the momentum in the radial direction to be negligible compared to the momentum in the axial and tangential direction. Taking the 3D Navier-Stokes equations and the continuity equation leaving out the momentum equation in the radial direction, replacing the pressure term with the hydrostatic pressure, and integrating momentum and continuity equations along the liquid height of each layer, and applying kinematic boundary condition on the free surface and at the interface between two layers one obtains the two layer 2D shallow water equations [10]. The two layer SWE are conditionally hyperbolic non-linear PDEs. In our case the range of parameters preserves hyperbolicity and for this reason, we calculate the fluxes using the approximate Riemann solver. The two layer SWE are coupled with the heat advection-diffusion equation containing the latent heat source term due to solidification. The heat diffusion is also solved with the appropriate thermal boundary conditions inside the mould and both end cores. The numerical simulation is performed with the industrial input parameters. Results are validated against pyrometer and thermo-camera measurements.

1. THEORY

1.1 Two layer shallow water equations

In the present paper, the two layer shallow water equations are derived only in one dimension namely the axial direction x (Fig. 1). By replacing the pressure term in the 2D Navier-Stokes equations for the axial and the radial direction with the hydrostatic pressure, applying the kinematic boundary condition at the free-surface and at the interface between each layer, and integrating both momentum equations and the continuity equation over the height of each liquid, one yields the set of two layer one dimensional shallow water equations in the axial direction. The hydrostatic pressure is equivalent to the centrifugal pressure. In the plane defined by the radial and the axial direction, the Coriolis force as a next fictitious force does not have any non-zero component, as long as the rotation axis is coincident with the mould axis. Therefore, the Coriolis force does not appear in the momentum equations. The continuity equations for the outer layer (denoted by subscript 1) and the intermediate layer (denoted by subscript 2) take the form

$$(h_1)_t + (h_1 u_1)_x = 0 \qquad (1)$$
$$(h_2)_t + (h_2 u_2)_x = 0 \qquad (2)$$

where h is the height of a layer, and u is the mass-flow averaged velocity of the corresponding layer. In this paper, the notation $(\cdot)_t$ stands for the partial time derivative and $(\cdot)_x$ for the derivative in x-direction. Note that since $h_1 + h_2 << R$, the axial and radial coordinates are mapped onto the Cartesian plane $\{x,r\} \rightarrow \{x,z\}$ as the following
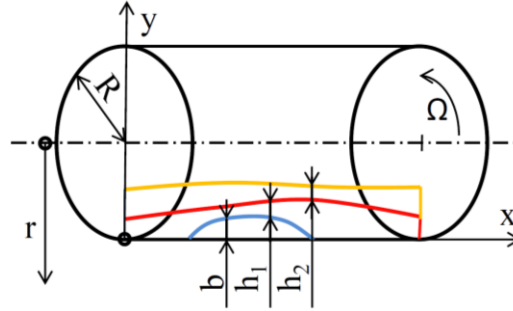
$$x = x \quad \text{and} \quad z = R - r \qquad (3)$$

Figure 1. Schematic of the HSC process depicting two liquid layers and solidified shell denoted by $h_1, h_2,$, and b, respectively.

The momentum equations for each layer are given by

$$(h_1 u_1)_t + \left(h_1 u_1^2 + \tfrac{1}{2} \Omega^2 R h_1^2 \right)_x =$$
$$-\Omega^2 R h_1(b)_x - \frac{\rho_1}{\rho_2} \Omega^2 R h_1(h_2)_x - \frac{\tau_b}{\rho_1} + \frac{\tau_i}{\rho_1} \qquad (4)$$

$$(h_2 u_2)_t + \left(h_2 u_2^2 + \tfrac{1}{2} \Omega^2 R h_2^2 \right)_x =$$
$$-\Omega^2 R h_2(b)_x - \frac{\rho_1}{\rho_2} \Omega^2 R h_2(h_1)_x - \frac{\tau_i}{\rho_2} \qquad (5)$$

with Ω the angular frequency of the mould, R the inner radius of the mould, b is the height of the solid layer growing from the mould wall, ρ the density of the liquid layer, τ_b and τ_i the bed shear stress and the shear stress between the layers both derived by assuming a parabolic velocity profiles in each layer. The bottom shear stress τ_b and the shear stress τ_i between the layers are expressed by the following formulas

$$\tau_b = 3 \frac{\mu_1}{h_1} u_1 \qquad (6)$$

$$\tau_i = 3 \frac{\mu_2}{h_2} \{u_2 - u_1\} \qquad (7)$$

The momentum exchange between two layers is thus realized through two mechanisms. The first mechanism is hydrostatic, meaning that any slope of the layer 1 will influence the layer 2 and vice versa. The second mechanism is kinetic,

meaning that the moving layer 1 will drag the layer 2 and vice versa. Note that the two layer SWE are only applicable when the density of the layer 1 is larger than the density of the layer 2 at the top $\rho_1 > \rho_2$. When $\rho_1 < \rho_2$ the heavier liquid at the top will penetrate the lighter liquid at the bottom via the mechanism of Kelvin-Helmholtz instability [11]. In the HSC process, it is naturally desired that the density of the outer layer ρ_1 is larger than the density of the intermediate layer ρ_2.

1.2 Heat advection equation for each layer
Due to the fact that the horizontal velocity field is solved by the SWE, the advection of the temperature field has to be solved correspondingly. In other words, the mass-flow averaged velocities u_1 and u_2 are used to advect the temperature field averaged over the height of each layer. For each layer we therefore solve the advection equation given by:

$$(h_1\overline{T}_1)_t + (h_1 u_1 \overline{T}_1)_x = 0 \qquad (8)$$
$$(h_2\overline{T}_2)_t + (h_2 u_2 \overline{T}_2)_x = 0 \qquad (9)$$

where $\overline{T}$ is the temperature averaged over the liquid height. Note that the heat advection is solved together with the two layer SWE. The heat diffusion inside layers, the mould, and the end cores is solved in a fractional step approach along with the solidification.

1.3 Heat diffusion, solidification, and mould filling
After the average flow dynamics is solved together with the heat advection in each layer, the heat diffusion is solved with the appropriate thermal boundary conditions (Table 1). A refractory coating applied in the contact between the casting and the mould is taken into account via a thin wall model. In order to correctly mimic the latent heat release due to the solidification, the source of the latent heat is added to the heat diffusion equation, which written in the cylindrical coordinates takes the following form:

$$\rho c_p (T)_t = \tfrac{1}{r}\big(k r (T)_r\big)_r - \rho L f_t \qquad (10)$$

with r the radial distance from the mould axis, k the thermal conductivity of the actual material, L the latent heat, and f the liquid fraction. The term with the latent heat is potentially a stiff

source term and special care has to be taken in order to avoid numerical instabilities and too expensive iterative algorithms. In the present paper we adopted an approach by Voller [12], which usually requires only a few iterations (~3) to converge the solution. For each layer a different liquid fraction-to-temperature relationship was used to mimic solidification of different materials (shown later in Sec. 3). After the temperature field is obtained, the solid height b is updated by using the new position of the solidification front corresponding to the isoline of solidus temperature. Note that the solid height b appears in the SWE, Eqs. (4)-(5).

The pouring of the outer and the intermediate layer is realized through the mass source term with the normal distribution placed in the mould centre. The initial momentum of newly incoming mass can be neglected when compared to the centrifugal pressure immediately exerted on the liquid body.

2. CALCULATION

All equations mentioned in Sec. 1 were solved in finite volume framework. The implicit backward Euler method [13] was applied to discretize the heat diffusion Eq. (10). The symmetric linear system of equations was solved with the help of the preconditioned conjugate gradient solver. The latent heat source term was split into an implicit and explicit part, which very much improved the convergence. Only a few iterations were necessary in order to drop residuals below the specified value.

Due to the hyperbolicity of the SWE, explicit updating formulas were used namely the first order Godunov's scheme with the high resolution corrections (MC limiter) [14]. The fluxes were determined from the approximate solution of the Riemann problem.

1.3 Approximate Riemann solver + fractional stepping
Symbolically, the SWE can be written as the following

$$Q_t + A(Q)_x = S \qquad (11)$$

where Q represents the vector of conserved quantities $Q = [h_1, h_1 u_1, h_1 \overline{T}_1, h_2, h_2 u_2, h_2 \overline{T}_2]^T$, A the vector of flux functions, and S the vector of

source terms. Eq. (11) can be rewritten in the following form

$$Q_t + A'(Q) \cdot Q_x = S \qquad (12)$$

where $A'(Q)$ is the Jacobian matrix with conditionally real eigenvalues. For the two layer SWE, a direct evaluation of the eigenspace is prohibitively very expensive. Instead, an approximation is more favourable. In the present paper, we expand about differences in the layer speeds and calculate first order approximations of eigenspeeds as

$$\lambda_{1,2} = \frac{h_1 u_1 + h_2 u_2}{h_1 + h_2} \pm \sqrt{\Omega^2 R\{h_1 + h_2\}} \qquad (13)$$

$$\lambda_{3,4} = \frac{h_1 u_1 + h_2 u_2}{h_1 + h_2}$$
$$\pm \sqrt{\frac{h_1 h_2}{h_1 + h_2}\left\{\left(1 - \frac{\rho_2}{\rho_1}\right)\Omega^2 R - \frac{\{u_2 - u_1\}^2}{h_1 + h_2}\right\}} \qquad (14)$$

$$\lambda_{5,6} = [u_1, u_2]^T \qquad (15)$$

where $\lambda_{1,2}$ and $\lambda_{3,4}$ represent the external and internal eigenspeeds, respectively. The external eigenspeeds correspond to the speeds of free-surface waves induced by the centrifugal pressure, whereas the internal waves are much smaller and correspond to waves due to the density and the velocity difference. The eigenspeeds $\lambda_{5,6}$ represent linearly degenerate waves passively carrying jumps in $h_1 T_1$ and $h_2 T_2$. From Eq. (14) the condition κ for the loss of hyperbolicity can be calculated

$$\kappa = \frac{\{u_2 - u_1\}^2}{\left\{1 - \frac{\rho_2}{\rho_1}\right\}\Omega^2 R\{h_1 + h_2\}} \leq 1 \qquad (16)$$

which is nearly the inverse of the Richardson number defining the transition to Kelvin-Helmholtz instability [15]. In the present paper, the hyperbolicity of Eq. (12) is however preserved and thus, an approximate Riemann solver can be used. By using the Jacobian matrix $A'(Q)$ from Eq. (12), the eigenvalues, Eqs. (13)-(14), and operation of linear algebra, the space of eigenvectors can be obtained. The following system of linear equations has to be solved for each eigenspeed λ in order to calculate corresponding columns of eigenvector space R.

$$A'(Q) \cdot [1, \alpha_1, \alpha_2, \alpha_3, \alpha_4, \alpha_5]^T = [1, \lambda\alpha_1, \lambda\alpha_2, \lambda\alpha_3, \lambda\alpha_4, \lambda\alpha_5]^T \qquad (17)$$

The final form of each of the eigenvectors is

$$r = [1, \lambda, T_1, \alpha_3, \lambda\alpha_4, \alpha_5 T_2]^T. \qquad (18)$$

Knowing the complete eigenspace of the hyperbolic system, Eq. (12), the strength of each wave α can be obtained by solving the linear system of equations [16]

$$R\alpha = \Delta Q \qquad (19)$$

with ΔQ being the jump of conserved quantities Q over the face of a finite volume element. After that, the fluxes can be obtained [17]. So far, only the homogeneous case of Eq. (11) was discussed $(S = 0)$. The first two terms on the right hand side of Eqs. (4) and (5) are upwinded by means of projecting it onto the matrix of eigenvectors and propagating it at the eigenspeeds, which result in a stationary discontinuity. Close to the numerical cells that are nearly empty it is crucial to apply a physical limit preventing from the occurrence of negative heights. The stationary discontinuity modifies the wave strengths of the homogeneous case, which in turn changes the resulting fluxes. A fractional stepping had to be applied for the remaining terms of the source S, namely all friction terms, as the following

$$(h_1 u_1)_t = -\frac{\tau_b}{\rho_1} + \frac{\tau_i}{\rho_1} \qquad (20)$$

$$(h_2 u_2)_t = -\frac{\tau_i}{\rho_2} \qquad (21)$$

The main reason for this is that it is not yet clear how to handle physical limits. As long as the friction terms stay weak compared to the convective and the centrifugal pressure terms, the fractional stepping will maintain a reasonable accuracy.

3. RESULTS AND DISCUSSION

The numerical model was verified against the pyrometer and the thermo-camera measurements conducted during the industrial HSC process. The important dimensions and the main process parameters are summarized in Table 1. The physical properties are listed in Table 2. The simulation was performed on a structured grid with around 20 000 volume elements. The calculation

was terminated by the user at 3300 s of physical time.

Table 1. Dimensions and process parameters

Parameter	value	unit
Length of mould	3.78	m
Inner radius of mould	0.424	m
Mass flow rate of outer layer	75	kg/s
Start of filling outer layer	0	s
Mass flow rate of outer layer	9.7	kg/s
Ambient temperature	25	°C
HTC[a] at outer surfaces	40	$W/m^2/K$
HTC at roller tracks	500	$W/m^2/K$

[a] heat transfer coefficient

Table 2. Physical properties of materials

	Outer layer	Intermediate layer	mould	end core	coating
Specific heat [J/kg/K]	430	450	490	650	
Thermal conductivity [$W/m^2/K$]	22	25	58.6	2.3	2.5
Density [kg/m^3]	7700	7200	7850	2200	
Latent heat [kJ/kg]	280	200	[a]		
Dynamic viscosity [Pa s]	0.006	0.006			

[a] blank entries are irrelevant i.e. not used in the numerical model

The simulation results were compared with the pyrometer and thermo-camera measurements. The pyrometer was used to record the free-surface temperature of the casting. The aiming position of the pyrometer was located approximately in 1/3rd of the mould length. In addition, the thermo-camera was recording the outer temperature of the mould. From the thermo-camera pictures the average temperature of the mould wall was calculated and used for the comparison. In Fig. 2, cooling curves from several castings of the same work roll obtained from the pyrometer are shown in thin solid lines. The cooling curve from the simulation is shown in a thick solid line. On a second y-axis, average temperatures of the external mould wall are compared. Simulation and experimental data are in a quite good agreement. Next, Fig. 3 shows the computational domain with the volume elements partially visible. At ~35 min., temperature contours are given along with important lines such as the free-surface line, the interface between the outer and intermediate layer, and isolines of liquidus and solidus temperatures.

In Fig. 3, the actual height h_2 of the intermediate layer is not uniform due to the intermediate layer spreading from the mould centre towards the end cores and the intermediate layer interacting with the outer layer through the friction and centrifugal pressure terms.
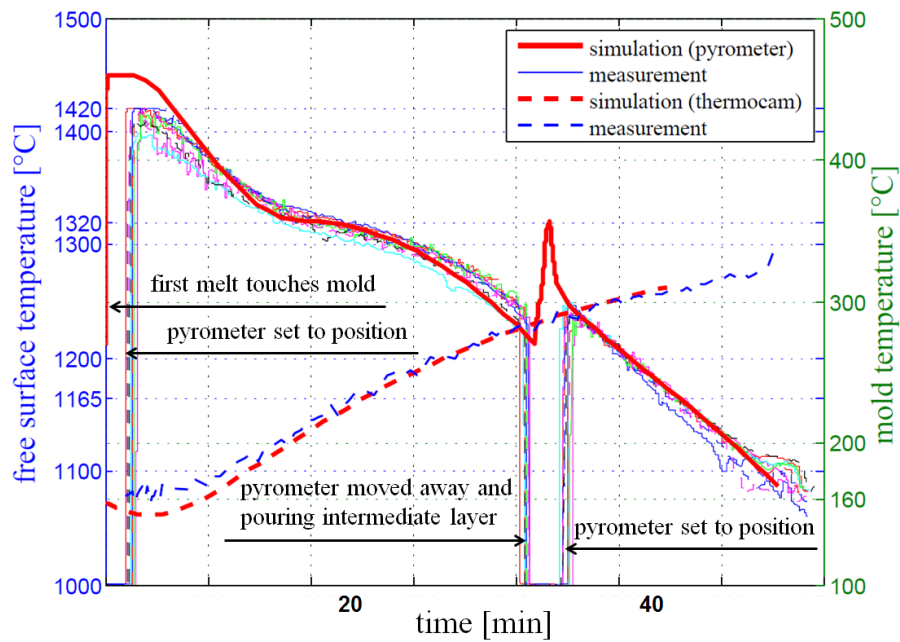
Figure 2. Comparison of cooling curves obtained from simulation and experiments (solid line – pyrometer, dashed line – thermo-camera).
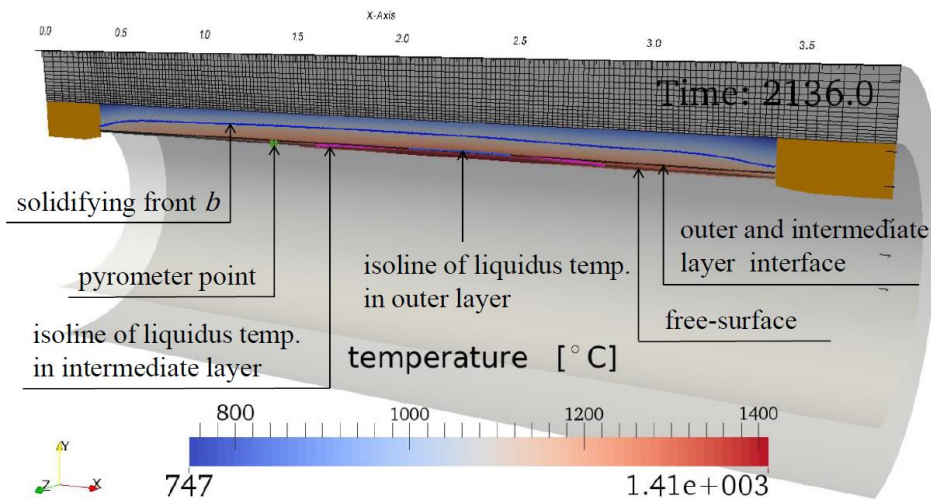

Figure 3. Temperature distribution in the outer and intermediate layer at ~35 min.

4. CONCLUSION

A simple algorithm was introduced allowing the calculation of the whole HSC process of the outer and intermediate layer of a work roll (~55 min) in a reasonable enough time, while still resolving main aspects of the flow. The Navier-Stokes equations were substituted by the two layer shallow water equations. The solidification (remelting) was solved with the help of the enthalpy method in finite volume framework considering the prescribed liquid fraction-to-temperature relationships. The numerical model was successfully verified against the pyrometer and thermo-camera measurements. The mixing due the density differences cannot be captured by the present approach, which can be marked as a main drawback of the model.

REFERENCES

[1] C.W. Hirt, and B.D. Nichols, J. Comp. Physics, 39 (1981) pp 201-225.

[2] Z. Xu, N. Song, R.V. Tol, Y. Luan and D. Li, Mater. Sci. Eng., 33 (2012) pp. 012030.

[3] E. Kaschnitz, Mater. Sci. Eng., 33 (2012) pp. 012031.

[4] K.S. Keerthiprasad, M.S. Murali, P.G. Mukunda and S. Majumdar, Metall. Mater. Trans.B, 42 (2010) pp 144-155.

[5] L. Drenchev, J. Sobczak, S. Malinoc and W. Sha, Modell. Sim. Mater. Sci. Eng., 11 (2003) pp 635-649.

[6] L. Drenchev, J. Sobczak, S. Malinoc and W. Sha, Modell. Sim. Mater. Sci. Eng., 11 (2003) pp 651-674

[7] N. Song, Y. Luan, Y. Bai, Z.A. Xu, X. Kang and D. Li, J. Mater. Sci. Tech., 28 (2012) pp 147-154.

[8] J. Bohacek, A. Kharicha, A. Ludwig and M. Wu, ISIJ Int., 54 (2014) pp 266-274.

[9] J. Bohacek, A. Kharicha, A. Ludwig and M. Wu, Mater. Sci. Eng., 33 (2013) pp. 012032.

[10] V.V. Ostapenko, J. Appl. Mech. Tech. Physics, 20 (1997) pp 127-135.

[11] W. Thomson, Phil. Mag., 42 (1871) pp 362-377.

[12] V.R. Voller and C.R. Swaminathan, Num. Heat Transfer B, 19 (1991) pp 175-189.

[13] J.C. Butcher: Numerical methods Ordinary Differential Equations, New York: John Wiley & Sons (2003)

[14] B. Van Leer, J. Comp. Physics, 23 (1977) pp 276-299.

[15] K.T. Mandli, PhD thesis, University. of Washington (2011) p 57.

[16] R.J. Leveque, Finite Volume Methods for Hyperbolic Problems, New York: Cambridge University Press (2002) p 54.

[17] D.L. George, PhD thesis University of Washington (2006) p 31